Chlorophyll Derivatives/MXene Hybrids for Photocatalytic Hydrogen Evolution: Dependence of Performance on the Central Coordinating Metals

Yuanlin Li[a], Tianfang Zheng[a], Yanxiang Liu[a], Yohan Dall'Agnese[b], Chunxiang Dall'Agnese[a], Cheng-Liang Liu[c], Shin-ichi Sasaki[d,e], Hitoshi Tamiaki[d] and Xiao-Feng Wang[a,*]

[a] *Key Laboratory of Physics and Technology for Advanced Batteries (Ministry of Education), College of Physics, Jilin University, Changchun 130012, PR China*

[b] *Institute for Materials Discovery, University College London, London WC1E 7JE, United Kingdom*

[c] *Department of Materials Science and Engineering, National Taiwan University, Taipei 10617, Taiwan*

[d] *Graduate School of Life Sciences, Ritsumeikan University, Kusatsu, Shiga 525-8577, Japan*

[e] *Nagahama Institute of Bio-Science and Technology, Nagahama, Shiga 526-0829, Japan*

*E-mail: xf_wang@jlu.edu.cn

Highlights

- Chl-*a* derivatives M-Chls with five different central ions, were used for HER.
- Noble metal-free photocatalytic system of M-Chls@$Ti_3C_2T_x$-based is developed.
- This work provides a way to synthesize environmentally friendly Chls for HER.

Table of Contents / Abstract Graphic

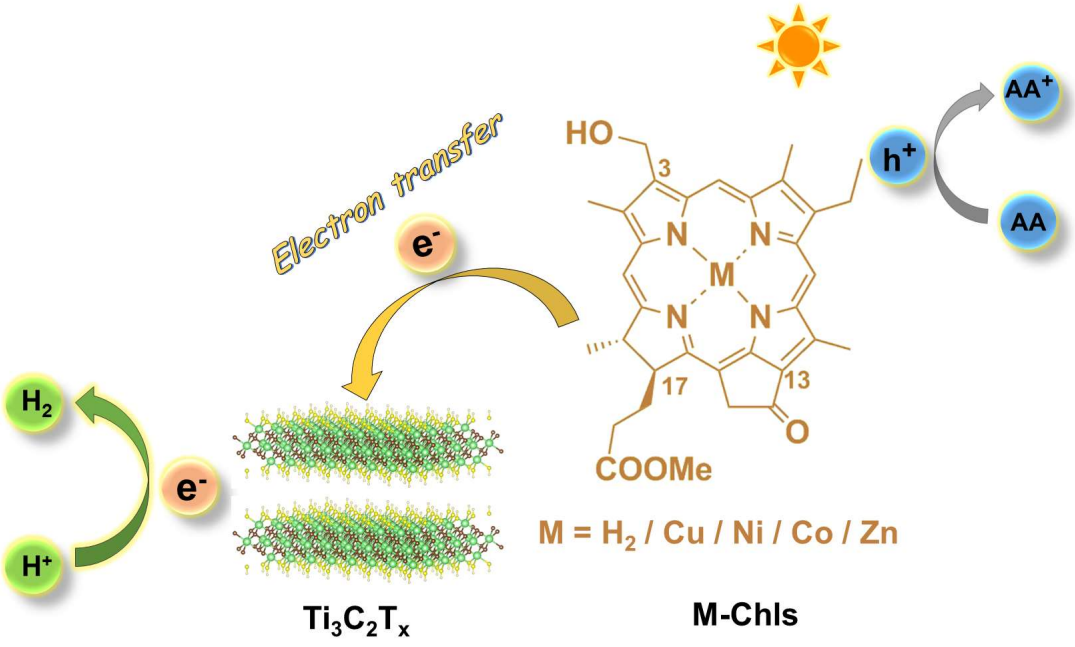

Abstract

Development of efficient photocatalytic hydrogen evolution reaction (HER) with illumination of visible light is challenging. In this work, five chlorophyll derivatives (M-Chls; M = H_2/Cu/Ni/Co/Zn) with different central ions in its cyclic tetrapyrrole ring including free base, copper, nickel, cobalt, and zinc were synthesized and employed as the effective visible-light harvester for efficient HER. In addition, 2D noble metal-free co-catalyst $Ti_3C_2T_x$ MXene was used as an excellent electron capturer due to its outstanding conductivity property. These M-Chls are modified on the surface of $Ti_3C_2T_x$ MXene with two-dimensional accordion-like morphology by means of a simple deposition process to form noble metal-free Chl/$Ti_3C_2T_x$-based photocatalysts for HER. It is found that the best HER performance as high as 49 μmol/h/g_{cat} was achieved with the Co-Chl@$Ti_3C_2T_x$ hybrid, which was much higher than those of other M-Chl@$Ti_3C_2T_x$ composites. This research provides a specific way to synthesize low-cost and environmentally friendly natural Chls for developing highly efficient photocatalytic HER through molecular engineering.

Keywords: central metals ion, chlorophyll derivatives, aggregates materials, hydrogen evolution reaction, $Ti_3C_2T_x$ MXene

1. Introduction

As an abundant, environmentally friendly, and renewable energy source, hydrogen energy has been considered as one of the most ideal potential candidates to replace traditional fossil energy sources, to meet the requirements of energy consumption[1-7].

Compared with other H_2 production strategies, the photocatalytic production of clean and renewable hydrogen is one of the extremely promising methods to solve the current energy and environmental issues by using freely available solar energy[8-12]. Over the past decades, considerable efforts have been made to explore various semiconductor photocatalysts, such as TiO_2[13,14], MoS_2[15-17], and C_3N_4[18-21]. However, after decades of efforts, the practical application of photocatalytic hydrogen evolution reactions (HERs) still has significant obstacles, such as insufficient absorption of visible light, poor hydrogen production efficiency, and high recombination efficiency of photo-generated electron-hole pairs which is mainly due to the sluggish kinetics on the catalyst surface[22].

Chlorophylls (Chls), the most abundant natural pigment, play an important role in light capture and energy transfer to the reaction centers in natural photosynthesis[23-26]. In recent years, Chls have witnessed widespread efforts in different systems, such as photoelectric conversion device[27-29], solar-driven photocatalytic hydrogen production[30-32], electrical energy storage device[33], and so on, due to the advantageous abundance of sources, cost-effectiveness, environmental friendliness, ease of dispose, and no toxicity[34-36]. However, pristine Chls have many shortcomings, such as insufficient ability of solar light absorption, high recombination efficiency of photoexcited electron-hole pairs, and inadequate active site, which limit their further application for highly efficient HER. In order to improve the photocatalytic activity, several studies have been carried out, such as elemental doping[37], co-catalyst loading[38] and molecular structure engineering[39]. Particularly, molecular structure

engineering of Chls has attracted increasing attention, owing to unique advantages that their chemical and physical properties are readily tunable. Thus, the exploration of Chl-based photocatalysts with well-designed molecular structures toward excellent catalytic performance is of high significance.

A new family of two-dimensional transition metal carbides and/or carbonitrides, called MXenes, was first reported in 2011[40]. MXenes are usually represented with the common formula $M_{n+1}X_nT_x$ (n = 1, 2, 3), where M, X and T represent the early transition metals element (Ti, Nb, V, Mo or Ta), carbon and/or nitrogen, and surface terminating group such as -F, -O and -OH, respectively[41]. $Ti_3C_2T_x$, as the most commonly used MXene, has been deeply investigated as co-catalyst in photocatalytic hydrogen production system[42-47]. This is mainly because it has multiple advantages, such as outstanding electrical conductivity, ultrathin 2D layered atomic structure, excellent hydrophilicity of the surface, and abundant surface active sites for reactions[48,49]. Consequently, $Ti_3C_2T_x$ MXene is an ideal candidate for promoting photocatalytic HER activity.

In the traditional MXenes-based photocatalytic system, photocatalyst is generally composed of inorganic semiconductors, while organic semiconductors remain largely unexplored. In our previous works, Chl aggregates as organic small molecule semiconductors were first employed with $Ti_3C_2T_x$ MXene as noble metal-free co-catalyst for HER, and we proved hydrogen generation through the exciton transfer in Chl aggregates followed by charge transfer to $Ti_3C_2T_x$[50]. However, the performance of this system was still insufficient and requires further improvement. With this in mind, in this

work, we propose a strategy by changing the central ion of Chls (M-Chls) in the cyclic tetrapyrrole through the molecular structure engineering. As a result, the photocatalytic performance of M-Chl@$Ti_3C_2T_x$ photocatalysts exhibited a significant improvement. We employed five M-Chls as photocatalysts with different central ions, namely, free base, copper, nickel, cobalt, and zinc methyl 3-devinyl-3-hydroxymethyl-pyropheophorbide-*a* (H_2/Cu/Ni/Co/Zn-Chl), that are combined with $Ti_3C_2T_x$ MXene as co-catalysts for photocatalytic activity study under the visible light irradiation ($\lambda > 420$ nm). We found that the Co-Chl@$Ti_3C_2T_x$ composite photocatalyst exhibited much higher photocatalytic performance than H_2/Cu/Ni/Zn-Chl@$Ti_3C_2T_x$ photocatalysts. This is mainly due the stronger light absorption ability, lower carrier recombination efficiency, lower transfer resistance, and higher photogenerated electron-hole pair separation efficiency of Co-Chl@$Ti_3C_2T_x$ than the other composites. This work may provide new perspectives on design of efficient Chl/$Ti_3C_2T_x$-based photocatalysts for photocatalytic hydrogen production.

2. Experimental section

2.1 Synthesis of Chls and $Ti_3C_2T_x$ MXene

M-Chls (M = H_2/Cu/Ni/Co/Zn) were prepared from chemical modification of naturally occurring Chl-*a* according to reported procedures[51,52].

$Ti_3C_2T_x$ MXene was obtained by etching Ti_3AlC_2 (Forsman, 98%) in 49% HF as follows. 49% HF (20 mL) was stirred at 300 rpm, and Ti_3AlC_2 (2 g) was slowly added to HF at room temperature for 24 h. After that, the obtained solution was washed and

centrifuged with deionized water several times until neutral pH was reached, then the $Ti_3C_2T_x$ sediment was collected after discarding the supernatant. Finally, $Ti_3C_2T_x$ MXene was dried in vacuum oven at 50 °C for 12 h.

2.2 Preparation of M-Chl@$Ti_3C_2T_x$ composites

$Ti_3C_2T_x$ (3 mg) and a certain amount of M-Chls were dissolved in tetrahydrofuran (THF). The mass ratios of M-Chls over $Ti_3C_2T_x$ were 0.5% (15 μg), 2% (60 μg), 4% (120 μg), or 8% (240 μg). Then, the M-Chl@$Ti_3C_2T_x$ mixtures were stirred at room temperature for 10 h until dry. Finally, M-Chl@$Ti_3C_2T_x$ composites was successfully prepared.

2.3 Characterization

To characterize M-Chls, $Ti_3C_2T_x$, and the composites, an X-ray diffractometer (XRD, D8 Advance, Bruker) was operated at 40 kV and 200 mA with Cu K_α radiation (λ = 0.15406 nm). Scanning electron microscopy (SEM, SU8000, Hitachi) was used to observe the morphology of the samples. Electronic absorption spectra of samples were measured with a UV-vis spectrometer (UV-3600, Shimadzu). The cyclic voltammograms (CV) were obtained on a VSP multichannel galvanostatic-potentiostatic system (Bio-Logic SAS, France).

2.4 Photocatalytic activity measurements

Photocatalytic H_2 evolution was measured under a 300 W Xenon lamp (PLS-SXE 300, Beijing Perfectlight Technology) with the light intensity of 100 mW/cm^2. A 6 mL photoreactor and a cut-off filter (usually λ > 420 nm) were used. M-Chl@$Ti_3C_2T_x$ photocatalysts (3 mg) were added in an aqueous 55 mM ascorbic acid (AA) solution (3

mL). The mixture was sonicated for 5 min before light irradiation to fully disperse the composites. Argon was purged to remove oxygen in the solution and the reactor for 10 min. The reactants were continuously stirred under irradiation of visible-to-near infrared light ($\lambda > 420$ nm) for 2 h. Then the hydrogen production was measured by a gas chromatograph (SP-3420A, Beijing Beifen-Ruili Analytical Instrument) with a thermal conductivity detector. The average values were obtained by five independent experiments. The carrier gas was argon and the column contained 5 Å molecular sieves.

2.5 Photoelectrochemical activity test

Electrochemical impedance spectroscopy (EIS) measurements in the range of 0.1 Hz to 100 kHz were carried out with an electrochemical workstation (Bio-Logic SAS) in a standard three-electrode system. The working electrode was prepared by ultrasonically dispersing the M-Chl@$Ti_3C_2T_x$ (M = H_2/Cu/Ni/Co/Zn) composites (10 mg) in a mixture of deionized water (250 μL), ethanol (250 μL) and Nafion solution (20 μL, Sigma-Aldrich, 5 wt%) for 5 min, then the dispersion (20 μL) was drop coated at room temperature onto an ITO square substrate (2 cm^2)[53]. Ag/AgCl was used as the reference electrode, and a Pt plate was used as the counter electrode. The electrolyte was an aqueous 0.5 M Na_2SO_4 solution containing AA (2 g/L). Transient photocurrent (TPC) responses were measured in the same three-electrode system. A 300 W Xenon lamp with a cut-off filter ($\lambda > 420$ nm) was used as the light source.

CV measurements were obtained by a three electrode system. M-Chls (M = H_2/Cu/Ni/Co/Zn) were dissolved in CH_2Cl_2 where 0.1 M tetrabutylammonium hexafluorophosphate ($TBAPF_6$) was used as the supporting electrolyte. Meanwhile, a

platinum wire was used as the working electrode and counter electrode, and Ag/AgCl was used as the reference electrode. The measurement potentials were calibrated with ferrocene/ferrocenium (Fc/Fc^{+}) redox couples. All measurements were conducted at room temperature.

3 Results and discussion

3.1 Structure and morphology

Scheme 1 shows the chemical structures of five M-Chls investigated in this work. These Chls have a cyclic tetrapyrrole as the framework and the same peripheral substituents, a hydroxymethyl group at the C3-position, a carbonyl group at the C13-position, and a methyl group as the esterifying moiety at the C17-propionate residue. Partial structural difference among them lies in the central ion in the cyclic tetrapyrrole ring, namely, M-Chls (M = H_2/Cu/Ni/Co/Zn) has a free base, copper, nickel, cobalt, and zinc as the central ion, respectively. It is worth mentioning that the 3^1-hydroxy group, central cobalt and zinc ion, and 13-carbonyl group along the molecular y-axis are of great significance for the self-assembly of M-Chls to form *J*-aggregates[51,52]. This is due to the coordination of the oxygen atom in the 3^1-hydroxy group with the central cobalt and zinc ion, and the formation of hydrogen bonds between the 3^1-hydroxy and the 13-carbonyl groups, thereby forming a strong intermolecular interaction of Co/Zn···O–H···O=C[51,52].

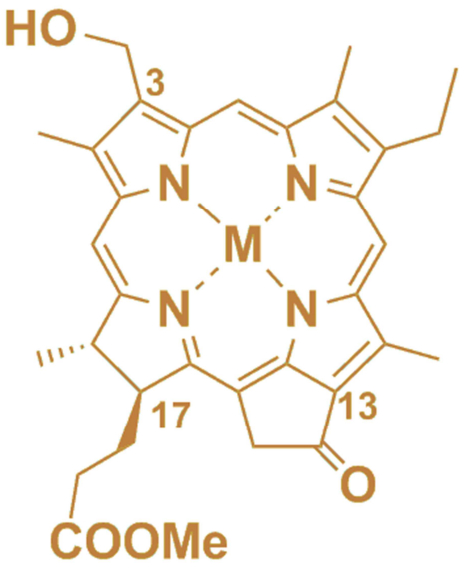

Scheme 1. Molecular structures of five Chl derivatives M-Chls in this study.

Figure 1a shows the schematic representation of the preparation process of M-Chl@$Ti_3C_2T_x$ composites. $Ti_3C_2T_x$ MXene was fabricated from its homologous MAX phase through selectively etching the Al-layers of Ti_3AlC_2 powder with HF. Then composites containing $Ti_3C_2T_x$ and different M-Chls were prepared and used as MXenes-based photocatalysts. Figure 1b shows the XRD patterns of the raw materials Ti_3AlC_2 before and after 24 h of etching. The (002) and (004) peaks of Ti_3AlC_2 moved toward low angles in $Ti_3C_2T_x$ and the most intense peak of Ti_3AlC_2 at 39.0° disappeared, indicating that the Ti_3AlC_2 was completely converted to $Ti_3C_2T_x$[54]. The corresponding SEM images of Ti_3AlC_2 before and after of etching are shown in Figures 1c and 1d, respectively. A typical 2D nanosheet accordion-like structure can be clearly observed in the HF-etched $Ti_3C_2T_x$.

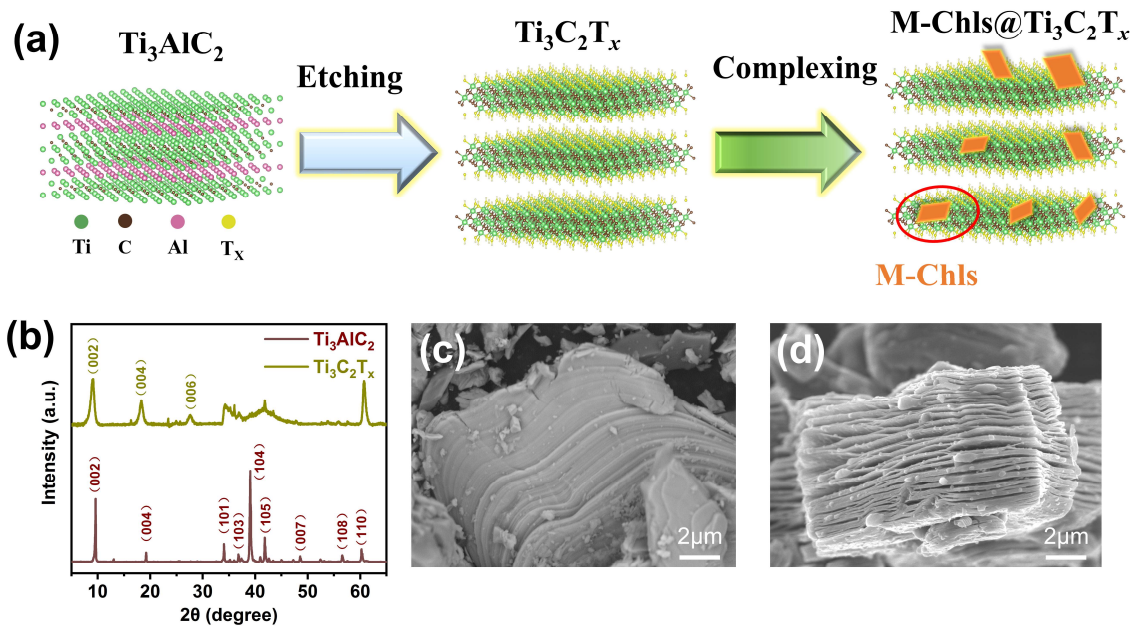

Figure 1. (a) Schematic diagram of the preparation process of M-Chl@$Ti_3C_2T_x$ composites, (b) XRD patterns of Ti_3AlC_2 (lower) and $Ti_3C_2T_x$ (upper), and SEM images of (c) Ti_3AlC_2 and (d) $Ti_3C_2T_x$.

3.2 Electronic absorption and electrochemical properties

To study the light absorption characteristics of the M-Chls and their composites, the electronic absorption spectra of M-Chls dissolved in THF and M-Chls@$Ti_3C_2T_x$ were illustrated in Figure 2a. The absorption spectra of H_2/Cu/Ni/Co/Zn-Chls in THF showed the redmost (Q_y) absorption bands at 672/662/658/675/670 nm and Soret peaks at 407/421/416/418/424 nm, respectively (broken lines in Figure 2a). Table 1 summarizes the relevant absorption parameters shown in Figure 2a. The sharp bands indicated that M-Chls were monomeric in THF. The electronic absorption spectra of M-Chl@$Ti_3C_2T_x$ photocatalysts only showed the characteristics of M-Chls, and no other absorption peaks are observed (solid line in Figure 2a). This is mainly due to the metallic property of

$Ti_3C_2T_x$, as previously reported[55]. The absorption spectra of M-Chl@$Ti_3C_2T_x$ composites showed obviously red-shifted and broadened Soret and Q_y absorption bands, compared with the corresponding monomeric M-Chls in THF. The Q_y absorption peaks H_2/Cu/Ni/Co/Zn-Chl@$Ti_3C_2T_x$ composites were located respectively at 696/681/673/716/720 nm, respectively. Such red shift and broadening would promote the charge transfer in aggregates. The considerable spectral changes are attributed to the *J*-aggregation of M-Chls by intermolecular π-π stacking. Furthermore, Co-Chl@$Ti_3C_2T_x$ showed a more red-shifted Q_y peak and a broader absorption band than the others, following the order of Co-Chl@$Ti_3C_2T_x$ > Zn-Chl@$Ti_3C_2T_x$ > > H_2-Chl@$Ti_3C_2T_x$ > Cu-Chl@$Ti_3C_2T_x$ > Ni-Chl@$Ti_3C_2T_x$.

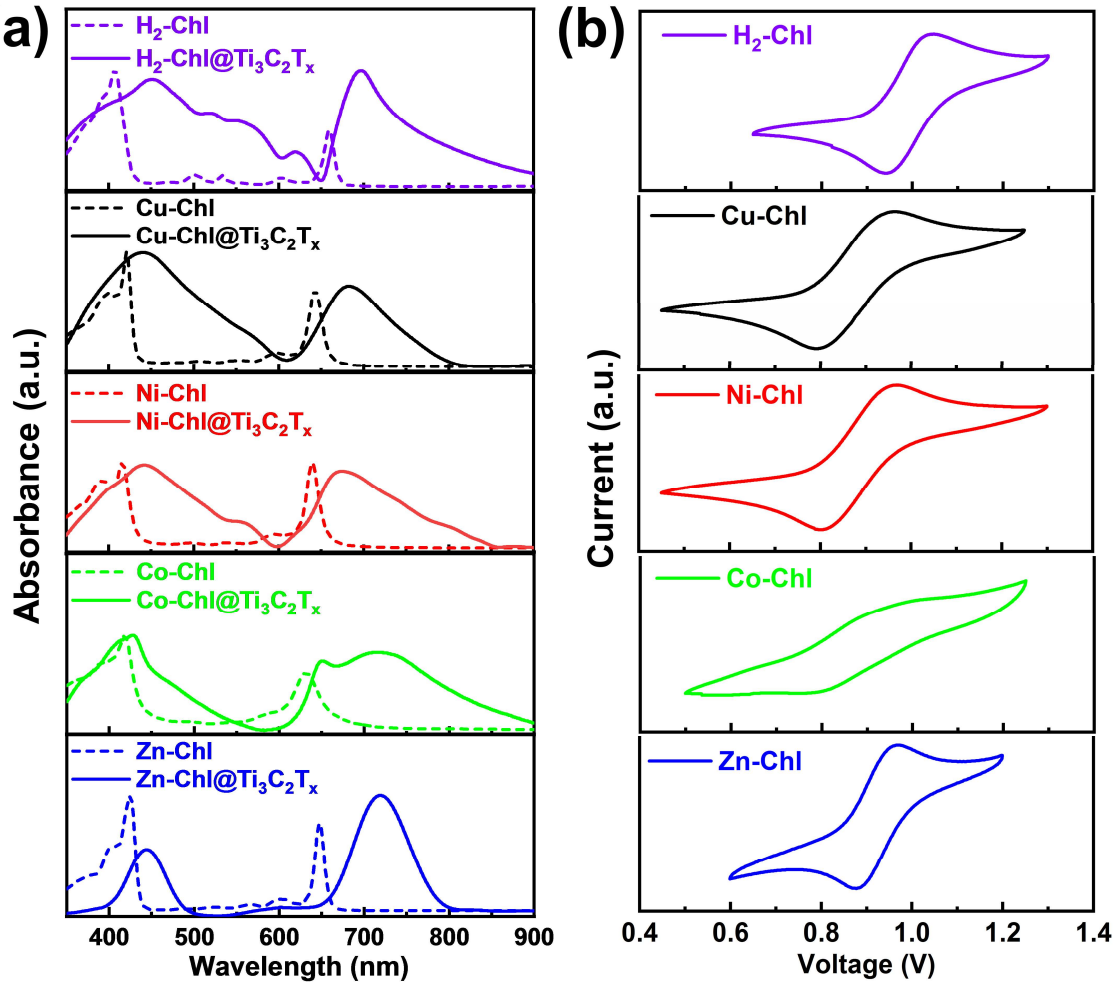

Figure 2. (a) Electronic absorption spectra of the five M-Chls in THF (broken lines) and the M-Chl@$Ti_3C_2T_x$ composites (solid lines) and (b) CVs of M-Chls with 0.1 M $TBAPF_6$ as a supporting electrolyte at a scan rate of 100 mV/s.

Table 1. Optoelectronic parameters for M-Chls.

M-Chls	λ_{Soret} [nm]	λ_{Qy} [nm]	E_g [eV]	E_{ox} [V]	HOMO [eV]	LUMO [eV]
H_2-Chl	407	672	1.85	0.92	-5.01	-3.16
Cu-Chl	421	662	1.87	0.79	-4.88	-3.01
Ni-Chl	416	658	1.88	0.80	-4.89	-3.01
Co-Chl	418	675	1.84	0.77	-4.86	-3.02
Zn-Chl	424	670	1.85	0.87	-4.96	-3.11

In order to investigate the electrochemical properties of M-Chls, the CVs of the five Chls in dichloromethane were measured, as shown in Figure 2b. The oxidation onset potentials (E_{ox}) of M-Chls (M = H_2, Cu, Ni, Co, and Zn) were 0.92, 0.79, 0.80, 0.77 and 0.87 V vs Ag/AgCl, respectively. The half-wave potential (E_{Fc}) of Fc/Fc^+ as an external reference was measured to be 0.71 V vs Ag/AgCl. The highest occupied molecular orbital (HOMO) energy levels of these molecules were estimated to be -5.01, -4.88, -4.89, -4.86 and -4.96 eV, respectively, from the following equation: HOMO (eV) = $-e(E_{ox} - E_{Fc} + 4.8)$. Their lowest unoccupied molecular orbital (LUMO) energy levels of M-Chls were also calculated following the equation: LUMO (eV) = HOMO + E_g, where E_g was the optical band gap obtained from the electronic absorption spectra: $E_g = 1240/\lambda_{Qy}$. The corresponding details are summarized in Table 1, and the values of LUMO are in the order

of Cu-Chl@$Ti_3C_2T_x$ = Ni-Chl@$Ti_3C_2T_x$ > Co-Chl@$Ti_3C_2T_x$ > Zn-Chl@$Ti_3C_2T_x$ > H_2-Chl@$Ti_3C_2T_x$, and the values of HOMO are in the order of Co-Chl@$Ti_3C_2T_x$ > Cu-Chl@$Ti_3C_2T_x$ > Ni-Chl@$Ti_3C_2T_x$ > Zn-Chl@$Ti_3C_2T_x$ > H_2-Chl@$Ti_3C_2T_x$. Due to the fact that the LUMO energy levels of all M-Chls are higher than the reduction potential of H_2/H^+, M-Chls are suitable as photocatalysts for water splitting. Meanwhile, the HOMO energy level of Co-Chl@$Ti_3C_2T_x$ is closer to the redox potential of AA, which may be one of the reasons for its higher photocatalytic activity.

3.3 Photocatalytic performance

In order to study the HER performances of as-prepared M-Chl@$Ti_3C_2T_x$ photocatalysts, these composites were tested for water splitting under the visible light (λ > 420 nm). Figure S1 shows the corresponding optimization details of mass ratio of M-Chls in the composites for photocatalytic hydrogen production. The optimized HER performances of M-Chls@$Ti_3C_2T_x$ are shown in Figure 3. It could be found that the best performance achieved was as high as 49 μmol/h/g_{cat} for the Co-Chl@$Ti_3C_2T_x$ composite, which was higher than those of H_2-Chl@$Ti_3C_2T_x$ (9 μmol/h/g), Cu-Chl@$Ti_3C_2T_x$ (31 μmol/h/g), Ni-Chl@$Ti_3C_2T_x$ (25 μmol/h/g) and Zn-Chl@$Ti_3C_2T_x$ (41 μmol/h/g) composites. This is mainly attributed to the strongest light-harvesting ability and highest electron-hole pair separation efficiency of Co-Chl@$Ti_3C_2T_x$ composite. Meanwhile, the previously reported hydrogen production efficiencies of MXene based composite photocatalysts were also compared and summarized in Table S1.

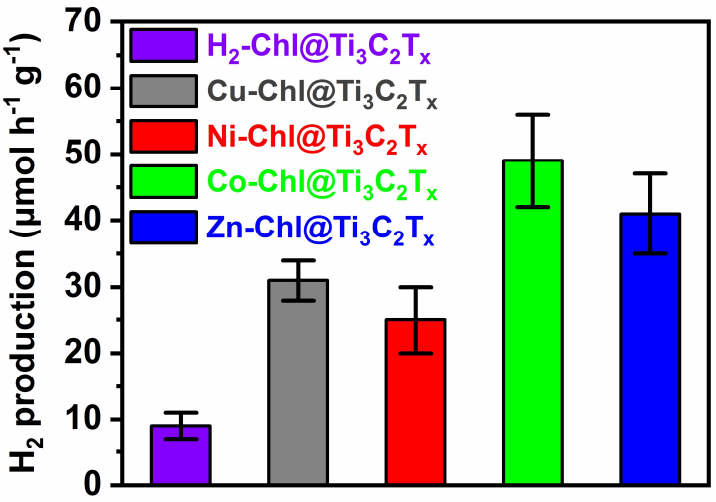

Figure 3. Optimized hydrogen production of M-Chl@$Ti_3C_2T_x$ composites: 4% H_2/Cu/Mn/Co-Chl@$Ti_3C_2T_x$ and 2% Zn-Chl@$Ti_3C_2T_x$

3.4 Photoelectrochemical measurements

EIS is an important way to evaluate the charge transfer resistance in the photocatalyst system. The smaller radius of the arc in the spectra indicates smaller electron transfer resistance between the surface of the photoelectrodes and electrolyte, which normally leads to more efficient separation of the photoelectron–hole pairs and faster interfacial charge transfer. The EIS Nyquist plots of aforementioned and the best-performed M-Chl@$Ti_3C_2T_x$ composites are illustrated in the Figure 4a and the corresponding equivalent model is displayed (inset). Here, R_1 and R_2 represent respectively the series resistance and the interfacial charge transfer resistance, CPE and W_0 are the constant phase element and the Warburg impedance, respectively[53]. The corresponding fitted data for the as-prepared samples are summarized in Table S2, and

the R_2 values follow the order of H_2-Chl@$Ti_3C_2T_x$ > Ni-Chl@$Ti_3C_2T_x$ > Cu-Chl@$Ti_3C_2T_x$ > Zn-Chl@$Ti_3C_2T_x$ > Co-Chl@$Ti_3C_2T_x$. The smaller radiuses of the semi-circles of Co/Zn-Chl@$Ti_3C_2T_x$ indicate that they possessed lower electron transfer resistance on the electrode surface and more efficient separation of photoelectron-hole pairs which would benefit the photocatalytic performance.

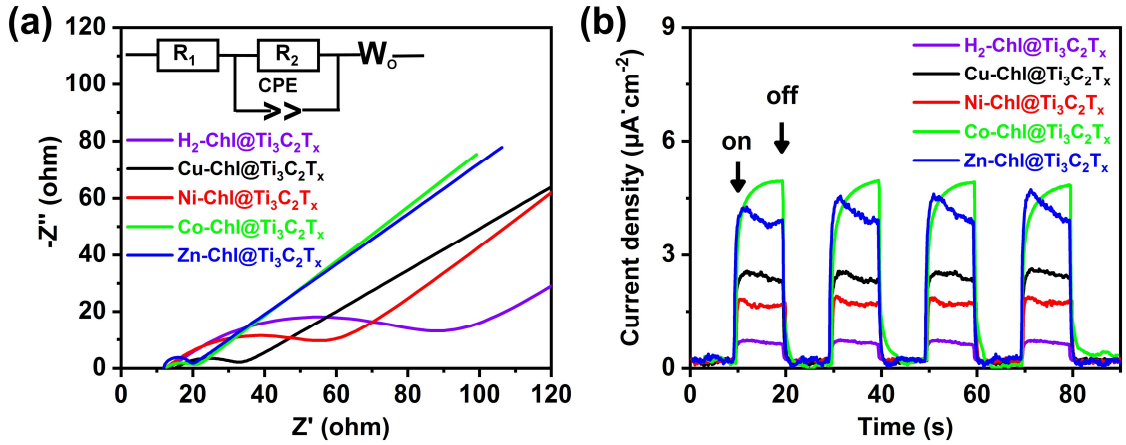

Figure 4. (a) EIS Nyquist plots and (b) TPC responses of the hybrids.

In order to reveal photo-induced charge separation and transfer processes, the TPC response were measured under visible light illumination (λ > 420 nm). As shown in Figure 4b, the photocurrent–time response of M-Chls@$Ti_3C_2T_x$ are prompt, steady, and reproducible with repeatable on/off cycles of light illumination. It could be seen that Co-Chl@$Ti_3C_2T_x$ and Zn-Chl@$Ti_3C_2T_x$ showed a much higher photocurrent than those of the other composites, indicating that they possessed stronger abilities of generating and transferring photogenerated electron-hole pairs which contributed to improved photocatalytic activity. Meanwhile, the Co-Chl@$Ti_3C_2T_x$ and Zn-Chl@$Ti_3C_2T_x$ curves showed some minor anomalies. The peak of Co-Chl@$Ti_3C_2T_x$ had a slow rise during the

photocurrent measurement, indicating that the photogenerated electron-hole pairs of Co-Chl@$Ti_3C_2T_x$ exhibited a tiny process for a hysteresis at the surface[56]. Additionally, the peak of Zn-Chl@$Ti_3C_2T_x$ showed generally minor decreased process. This is mainly attributed to photo-generated holes that are not completely consumed, which causes their recombination with electrons again[57].

Due to the higher LUMO energy levels of the M-Chls than the reduction potential of H_2/H^+, M-Chls are suitable for water splitting as photocatalysts. Furthermore, the best performance of Co-Chl@$Ti_3C_2T_x$ composite in HER systems can be attributed mainly to the following factors. First, based on the absorption spectrum, Co-Chl@$Ti_3C_2T_x$ showed an excellent intrinsic light gathering ability. Second, Co-Chl@$Ti_3C_2T_x$ showed a much smaller charge transfer resistance than the other composites, indicating that photogenerated electrons were more easily transferred from Co-Chl to $Ti_3C_2T_x$ for the HER with H^+ in the aqueous solution. Third, Co-Chl@$Ti_3C_2T_x$ showed the highest TPC response, indicating that it possesses the best photogenerated electron-hole pair separation ability.

3.5 Photocatalytic mechanism

The hydrogen generation process including the ways of transmission and separation of photoexcited electron-hole pairs in the M-Chl@$Ti_3C_2T_x$ composites is illustrated in Figure 5a. M-Chls are excited from HOMO to LUMO energy level when exposed to visible-to-near infrared light ($\lambda > 420$ nm). Meanwhile, electrons-hole pairs are generated, and then the photogenerated electrons can be transferred rapidly from the LUMO of M-

Chls to $Ti_3C_2T_x$ due to its excellent electronic conductivity. Consequently, two protons in the aqueous solution are efficiently reduced to produce H_2 by the accumulated electrons on the surface of $Ti_3C_2T_x$ thanks to its excellent capability for HER. Then, the holes of M-Chls can be reduced by obtaining an electron from the electron donor AA. So that, the photocatalyst M-Chls accomplish the cycle from excited state to ground state. Figure 5b displays the energy level diagram of the M-Chl@$Ti_3C_2T_x$ composites in this investigation. As previously reported, the work function of $Ti_3C_2T_x$ and redox potential of AA are -5.28 eV and -4.55 eV, respectively[58,59]. Thereby, the photoexcitation-induced electron/hole transfer can take place between M-Chls and $Ti_3C_2T_x$/AA. Importantly, the LUMO levels of M-Chls are sufficiently above that of H_2/H^+, indicating that M-Chls are suitable for HER as a light-absorption materials.

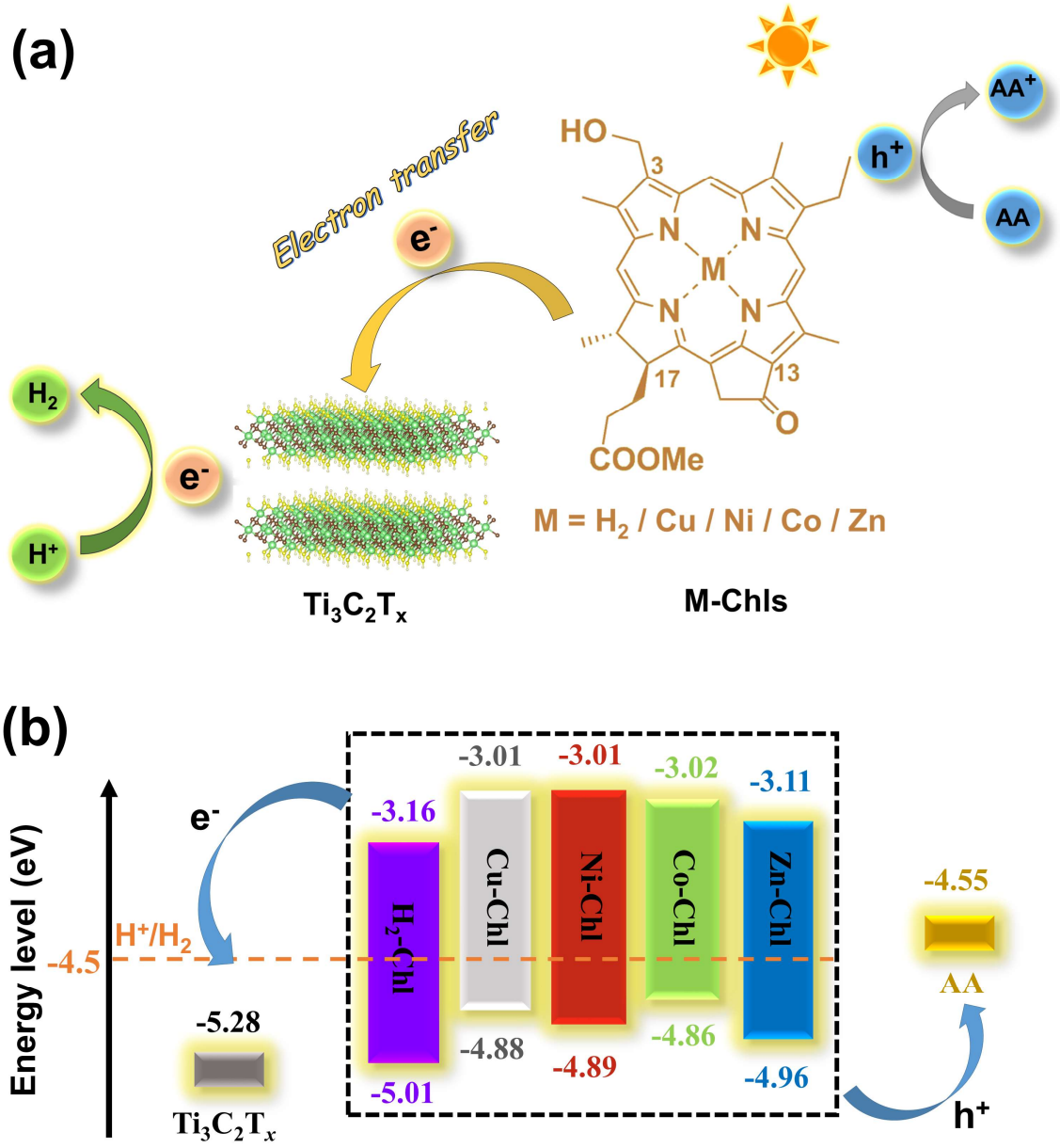

Figure 5. (a) Schematic diagram of hydrogen production of M-Chl@$Ti_3C_2T_x$ composites under visible light irradiation and (b) energy level diagram of the five M-Chls as photocatalyst.

4. Conclusion

In conclusion, Chl-*a* derivatives M-Chls with five different central ions (M = H_2/Cu/Ni/Co/Zn), were used for photocatalytic H_2 evolution as light-absorption materials in this work. Noble metal-free photocatalyst of M-Chls@$Ti_3C_2T_x$ were successfully synthesized by means of a simple deposition process. In this structure, natural pigments M-Chls act as the effective visible light harvester and ultrathin $Ti_3C_2T_x$ nanosheets act as an excellent electronic capturer. The optimal sample of 4% Co-Chl@$Ti_3C_2T_x$ showed the highest photocatalytic activity, as high as 49 μmol/h/g_{cat}, among the M-Chls, which can be interpreted with the stronger light capture ability, lower carrier recombination efficiency, lower transfer resistance, and higher photogenerated electron-hole pair separation efficiency of Co-Chl@$Ti_3C_2T_x$ than the others. This work provides a feasible strategy for the development of Chl/$Ti_3C_2T_x$-based photocatalyst systems under visible light with a high efficiency and a simple deposition method. Furthermore, this investigation offers guidelines for the synthesis of suitable Chls for efficient photocatalytic HER with Chl/MXene hybrid structures through molecular engineering.

Conflicts of interest

There are no conflicts to declare.

Acknowledgements

This work was supported by the National Natural Science Foundation of China (No. 11974129 to X.-F. W.) and "the Fundamental Research Funds for the Central Universities, Jilin University" and Japan Society for the Promotion of Science (JSPS) KAKENHI Grant Number JP17H06436 (to H.T.).

References

[1] Acar C, Dincer I, Naterer GF. Review of photocatalytic water-splitting methods for sustainable hydrogen production. Int J Energy Res. 2016;40:1449-73.

[2] Pan H. Principles on design and fabrication of nanomaterials as photocatalysts for water-splitting. Renewable Sustainable Energy Rev. 2016;57:584-601.

[3] Wu HB, Xia BY, Yu L, Yu XY, Lou XW. Porous molybdenum carbide nano-octahedrons synthesized via confined carburization in metal-organic frameworks for efficient hydrogen production. Nat Commun. 2015;6:6512.

[4] Pan H, Qiu XF, Ivanovc IN, Meyer HM, Wang W, Zhu WG, Paranthaman MP, Zhang ZY, Eres G, Gu BH. Fabrication and characterization of brookite-rich, visible light-active TiO_2 films for water splitting. Appl Catal B. 2009;93:90-5.

[5] Voloshin RA, Bedbenov VS, Gabrielyan DA, Brady NG, Kreslavski VD, Zharmukhamedov SK, Rodionova MV, Bruce BD, Allakhverdiev SI. Optimization and characterization of TiO_2-based solar cell design using diverse plant pigments. Int J Hydrogen Energy. 2017;42:8576-85.

[6] Voloshin RA, Rodionova MV, Zharmukhamedov SK, Nejat Veziroglu T,

Allakhverdiev SI. Review: biofuel production from plant and algal biomass. Int J Hydrogen Energy. 2016;41:17257-73.

[7] Rodionova MV, Poudyal RS, Tiwari I, Voloshin RA, Zharmukhamedov SK, Nam HG, Zayadan BK, Bruce BD, Hou HJM, Allakhverdiev SI. Biofuel production: challenges and opportunities. Int J Hydrogen Energy. 2017;42:8450-61.

[8] Yu XY, Feng Y, Jeon Y, Guan B, Lou XW, Paik U. Formation of Ni-Co-MoS_2 nanoboxes with enhanced electrocatalytic activity for hydrogen evolution. Adv Mater. 2016;28:9006-11.

[9] Yu L, Xia BY, Wang X, Lou XW. General formation of M-MoS_3 (M = Co, Ni) hollow structures with enhanced electrocatalytic activity for hydrogen evolution. Adv Mater. 2016;28:92-7.

[10] Pan H, Zhang YW. GaN/ZnO superlattice nanowires as photocatalyst for hydrogen generation: A first-principles study on electronic and magnetic properties. Nano Energy. 2012;1:488-93.

[11] Ma FX, Wu HB, Xia BY, Xu CY, Lou XW. Hierarchical beta-Mo_2C nanotubes organized by ultrathin nanosheets as a highly efficient electrocatalyst for hydrogen production. Angew Chem Int Ed. 2015;54:15395-9.

[12] Ma XR, Dang R, Yang N, Li X, Zhang Y, Gong Y, Liu ZP, Guo W, Zhang YY, Li CY. Anchoring single Pt atoms on hollow Ag_3VO_4 spheres for improved activity towards photocatalytic H_2 evolution reaction. Int J Hydrogen Energy. 2021;46:22842-51.

[13] Lang XJ, Ma WH, Chen CC, Ji HW, Zhao JC. Selective aerobic oxidation mediated

by TiO_2 photocatalysis. Acc Chem Res. 2014;47:355-63.

[14] Ma Y, Wang XL, Jia YS, Chen XB, Han HX, Li C. Titanium dioxide-based nanomaterials for photocatalytic fuel generations. Chem Rev. 2014;114:9987-10043.

[15] Peng R, Liang LB, Hood ZD, Boulesbaa A, Puretzky A, Ievlev AV, Come J, Ovchinnikova OS, Wang H, Ma C, Chi MF, Sumpter BG, Wu ZL. In-plane heterojunctions enable multiphasic two-dimensional (2D) MoS_2 nanosheets as efficient photocatalysts for hydrogen evolution from water reduction. ACS Catal. 2016;6:6723-9.

[16] Krishnan U, Kaur M, Singh K, Kumar M, Kumar A. A synoptic review of MoS_2: Synthesis to applications. Superlattices Microst. 2019;128:274-97.

[17] Yuan Y, Guo R-t, Hong L-f, Ji X-y, Li Z-s, Lin Z-d, Pan W-g. Recent advances and perspectives of MoS_2-based materials for photocatalytic dyes degradation: A review. Colloids Surf A. 2021;611:125836.

[18] Ong WJ, Tan LL, Ng YH, Yong ST, Chai SP. Graphitic carbon nitride (g-C_3N_4)-based photocatalysts for artificial photosynthesis and environmental remediation: are we a step closer to achieving sustainability? Chem Rev. 2016;116:7159-329.

[19] Cao SW, Yu JG. g-C_3N_4-based photocatalysts for hydrogen generation. J Phys Chem Lett. 2014;5:2101-7.

[20] Zheng DD, Cao XN, Wang XC. Precise formation of a hollow carbon nitride structure with a Janus surface to promote water splitting by photoredox catalysis. Angew Chem Int Ed. 2016;55:11512-6.

[21] Sun JH, Zhang JS, Zhang MW, Antonietti M, Fu XZ, Wang XC. Bioinspired hollow semiconductor nanospheres as photosynthetic nanoparticles. Nat Commun.

2012;3:1139.

[22] Bai S, Zhang N, Gao C, Xiong Y. Defect engineering in photocatalytic materials. Nano Energy. 2018;53:296-336.

[23] Qiu NW, Jiang DC, Wang XS, Wang BS, Zhou F. Advances in the members and biosynthesis of chlorophyll family. Photosynthetica. 2019;57:974-84.

[24] Tamiaki H, Shibata R, Mizoguchi T. The 17-propionate function of (bacterio)chlorophylls: biological implication of their long esterifying chains in photosynthetic systems. Photochem Photobiol. 2007;83:152-62.

[25] Ryan AA, Senge MO. How green is green chemistry? Chlorophylls as a bioresource from biorefineries and their commercial potential in medicine and photovoltaics. Photochem Photobiol Sci. 2015;14:638-60.

[26] Voloshin RA, Brady NG, Zharmukhamedov SK, Feyziyev YM, Huseynova IM, Najafpour MM, Shen JR, Veziroglu TN, Bruce BD, Allakhverdiev SI. Influence of osmolytes on the stability of thylakoid-based dye-sensitized solar cells. Int J Energy Res. 2019.

[27] Wang B, Li N, Yang L, Dall'Agnese C, Jena AK, Sasaki S, Miyasaka T, Tamiaki H, Wang X-F. Chlorophyll derivative-sensitized TiO_2 electron transport layer for record efficiency of $Cs_2AgBiBr_6$ double perovskite solar cells. J Am Chem Soc. 2021;143:2207-11.

[28] Duan S, Dall'Agnese C, Chen G, Wang X-F, Tamiaki H, Yamamoto Y, Ikeuchi T, Sasaki S. Bilayer chlorophyll-based biosolar cells inspired from the Z-scheme process of oxygenic photosynthesis. ACS Energy Lett. 2018;3:1708-12.

[29] Li M, Li Y, Sasaki S, Song J, Wang C, Tamiaki H, Tian W, Chen G, Miyasaka T, Wang X-F. Dopant-free zinc chlorophyll aggregates as an efficient biocompatible hole transporter for perovskite solar cells. ChemSusChem. 2016;9:2862-9.

[30] Li Y, Sun Y, Zheng T, Dall'Agnese Y, Dall'Agnese C, Meng X, Sasaki S, Tamiaki H, Wang X-F. Chlorophyll-based organic heterojunction on $Ti_3C_2T_x$ MXene nanosheets for efficient hydrogen production. Chem Eur J. 2021;27:5277-82.

[31] Sun Y, Wang X-F, Chen G, Zhan CH, Kitao O, Tamiaki H, Sasaki S. Near-infrared absorption carboxylated chlorophyll-*a* derivatives for biocompatible dye-sensitized hydrogen evolution. Int J Hydrogen Energy. 2017;42:15731-8.

[32] Sun Y, Sun Y, Dall'Agnese C, Wang X-F, Chen G, Kitao O, Tamiaki H, Sakai K, Ikeuchi T, Sasaki S. Dyad sensitizer of chlorophyll with indoline dye for panchromatic photocatalytic hydrogen evolution. ACS Appl Energy Mater. 2018;1:2813-20.

[33] Zhang C, Zhao W, Sasaki S, Tamiaki H, Wang X-F. A chlorophyll derivative-based bio-solar energy conversion and storage device. Electrochim Acta. 2020;347:136283.

[34] Li Y, Sasaki S, Tamiaki H, Liu CL, Song JX, Tian WJ, Zheng EQ, Wei YJ, Chen G, Fu XQ, Wang X-F. Zinc chlorophyll aggregates as hole transporters for biocompatible, natural-photosynthesis-inspired solar cells. J Power Sources. 2015;297:519-24.

[35] Sasaki S, Wang X-F, Ikeuchi T, Tamiaki H. Synthesis of carboxylated chlorophylls and their application as functional materials. J Porphyrins Phthalocyanines. 2015;19:517-26.

[36] Duan S, Zhou Q, Li AJ, Wang X-F, Sasaki S, Tamiaki H. Semisynthetic chlorophyll derivatives toward solar energy applications. Sol RRL. 2020;4.

[37] Lin ZZ, Wang XC. Nanostructure engineering and doping of conjugated carbon nitride semiconductors for hydrogen photosynthesis. Angew Chem Int Ed. 2013;52:1735-8.

[38] Bi LL, Meng DD, Bu QJ, Lin YH, Wang DJ, Xie TF. Electron acceptor of Ni decorated porous carbon nitride applied in photocatalytic hydrogen production. Phys Chem Chem Phys. 2016;18:31534-41.

[39] Zhang JY, Wang YH, Jin J, Zhang J, Lin Z, Huang F, Yu JG. Efficient visible-light photocatalytic hydrogen evolution and enhanced photostability of core/shell CdS/g-C_3N_4 nanowires. ACS Appl Mater Interfaces. 2013;5:10317-24.

[40] Naguib M, Kurtoglu M, Presser V, Lu J, Niu JJ, Heon M, Hultman L, Gogotsi Y, Barsoum MW. Two-dimensional nanocrystals produced by exfoliation of Ti_3AlC_2. Adv Mater. 2011;23:4248-53.

[41] Naguib M, Mochalin VN, Barsoum MW, Gogotsi Y. 25th anniversary article: MXenes: a new family of two-dimensional materials. Adv Mater. 2014;26:992-1005.

[42] Huang KL, Li CH, Li HZ, Ren GM, Wang L, Wang WT, Meng XC. Photocatalytic applications of two-dimensional Ti_3C_2 MXenes: a review. ACS Appl Nano Mater. 2020;3:9581-603.

[43] Zhang JH, Xing C, Shi F. MoS_2/Ti_3C_2 heterostructure for efficient visible-light photocatalytic hydrogen generation. Int J Hydrogen Energy. 2020;45:6291-301.

[44] Xiao R, Zhao C, Zou Z, Chen Z, Tian L, Xu H, Tang H, Liu Q, Lin Z, Yang X. In situ fabrication of 1D CdS nanorod/2D Ti_3C_2 MXene nanosheet schottky heterojunction toward enhanced photocatalytic hydrogen evolution. Appl Catal B. 2020;268:118382.

[45] Xu H, Xiao R, Huang J, Jiang Y, Zhao C, Yang X. In situ construction of protonated g-C_3N_4/Ti_3C_2 MXene Schottky heterojunctions for efficient photocatalytic hydrogen production. Chinese J Catal. 2021;42:107-14.

[46] Prasad C, Yang X, Liu Q, Tang H, Rammohan A, Zulfiqar S, Zyryanov GV, Shah S. Recent advances in MXenes supported semiconductors based photocatalysts: properties, synthesis and photocatalytic applications. J Ind Eng Chem. 2020;85:1-33.

[47] Ding M, Xiao R, Zhao C, Bukhvalov D, Chen Z, Xu H, Tang H, Xu J, Yang X. Evidencing interfacial charge transfer in 2D CdS/2D MXene schottky heterojunctions toward high-efficiency photocatalytic hydrogen production. Sol RRL. 2020;5:2000414.

[48] Anasori B, Lukatskaya MR, Gogotsi Y. 2D metal carbides and nitrides (MXenes) for energy storage. Nat Rev Mater. 2017;2:16098.

[49] Lukatskaya MR, Mashtalir O, Ren CE, Dall'Agnese Y, Rozier P, Taberna PL, Naguib M, Simon P, Barsoum MW, Gogotsi Y. Cation intercalation and high volumetric capacitance of two-dimensional titanium carbide. Science. 2013;341:1502-5.

[50] Li Y, Chen X, Sun Y, Meng X, Dall'Agnese Y, Chen G, Dall'Agnese C, Ren H, Sasaki S, Tamiaki H, Wang X-F. Chlorosome-like molecular aggregation of chlorophyll derivative on $Ti_3C_2T_x$ MXene nanosheets for efficient noble metal-free photocatalytic hydrogen evolution. Adv Mater Interfaces. 2020;7:1902080.

[51] Tamiaki H, Amakawa M, Shimono Y, Tanikaga R, Holzwarth AR, Schaffner K. Synthetic zinc and magnesium chlorin aggregates as models for supramolecular antenna complexes in chlorosomes of green photosynthetic bacteria. Photochem Photobiol. 1996;63:92-9.

[52] Tamiaki H, Amakawa M, Holzwarth AR, Schaffner K. Aggregation of synthetic metallochlorins in hexane. A model of chlorosomal bacteriochlorophyll self-assemblies in green bacteria. Photosynth Res. 2002;71:59-67.

[53] Su T, Peng R, Hood ZD, Naguib M, Ivanov IN, Keum JK, Qin Z, Guo Z, Wu Z. One-step synthesis of Nb_2O_5/C/Nb_2C (MXene) composites and their use as photocatalysts for hydrogen evolution. ChemSusChem. 2018;11:688-99.

[54] Cao SW, Shen BJ, Tong T, Fu JW, Yu JG. 2D/2D heterojunction of ultrathin MXene/Bi_2WO_6 nanosheets for improved photocatalytic CO_2 reduction. Adv Funct Mater. 2018;28:1800136.

[55] Ran J, Gao G, Li FT, Ma TY, Du A, Qiao SZ. Ti_3C_2 MXene co-catalyst on metal sulfide photo-absorbers for enhanced visible-light photocatalytic hydrogen production. Nat Commun. 2017;8:13907.

[56] Covington LR, Moore JC. Photoconductivity and transient response of Al:ZnO:Al planar structures fabricated via a thermal oxidation process. Thin Solid Films. 2013;540:106-11.

[57] Zhang LW, Zhang YM, Huang XJ, Tao LM, Bi YP. Direct observation of dynamic interfacial bonding and charge transfer in metal-free photocatalysts for efficient hydrogen evolution. Appl Catal B. 2021;283:119633.

[58] Yang L, Dall'Agnese Y, Hantanasirisakul K, Shuck CE, Maleski K, Alhabeb M, Chen G, Gao Y, Sanehira Y, Jena AK, Shen L, Dall'Agnese C, Wang X-F, Gogotsi Y, Miyasaka T. SnO_2-Ti_3C_2 MXene electron transport layers for perovskite solar cells. J Mater Chem A. 2019;7:5635-42.

[59] Cardoso JC, Stulp S, de Souza MKR, Hudari FF, Gubiani JR, Frem RCG, Zanoni MVB. The effective role of ascorbic acid in the photoelectrocatalytic reduction of CO_2 preconcentrated on TiO_2 nanotubes modified by ZIF-8. J Electroanal Chem. 2020;856:113384.